Journal of Physics:
Conference Series

PAPER • **OPEN ACCESS**

Cryo-cooled silicon monochromators at the Materials Imaging and Dynamics (MID) instrument of the European XFEL

To cite this article: A.V. Zozulya *et al* 2025 *J. Phys.: Conf. Ser.* **3010** 012057

Journal of Physics: Conference Series **3010** (2025) 012057 doi:10.1088/1742-6596/3010/1/012057

Cryo-cooled silicon monochromators at the Materials Imaging and Dynamics (MID) instrument of the European XFEL

A.V. Zozulya[1], L. Samoylova[1], U. Bösenberg[1], J. Hallmann[1], W. Jo[1], J.Möller[1], J.-E. Pudell[1], A. Rodriguez-Fernandez, T. Roth[2], R. Shayduk[1], H. Sinn[1], D. Shu[3], M. Dommach[1], J. Eidam[1], M. Vannoni[1] and A. Madsen[1]

[1] European X-ray Free-Electron Laser Facility, Schenefeld, Germany
[2] European Synchrotron Radiation Facility, Grenoble, France
[3] ANL, Argonne, Illinois, United States

*E-mail: alexey.zozulya@xfel.eu

Abstract. Monochromatization and diagnostics of SASE spectral properties over the entire hard X-ray range are important for many experiments utilizing transverse and longitudinal coherence of XFEL beam. For this purpose the Materials Imaging and Dynamics instrument at European XFEL is equipped with two cryo-cooled double-crystal monochromators using Si111 and Si220 optics. Optical parameters, design and performance of both monochromators are presented.

1. Introduction

The advent of X-ray Free-Electron Laser (XFEL) sources producing ultrashort X-ray pulses opened up unexplored experimental areas in both fundamental and applied research [1, 2]. The European XFEL (EuXFEL) is a worldwide unique facility based on superconducting accelerator technology and the self-amplified spontaneous emission (SASE) process to generate X-ray pulses at MHz repetition rates [3]. EuXFEL operates simultaneously at three undulator branches SASE1, SASE2 and SASE3. Extra-long beam transport distances (about 1 km) and high peak power apply rigid requirements to X-ray optics and diagnostics components delivering XFEL beams to experimental stations [4]. The Materials Imaging and Dynamics (MID) instrument [5] is located at the SASE2 undulator sharing common upstream beam transport components with HED instrument [4]. The MID instrument provides versatile setups for user experiments employing X-ray photon correlation spectroscopy, coherent X-ray diffraction imaging, high resolution scattering, and ultrafast pump-probe techniques [6]. Among other beam parameters, monochromatization of the SASE spectrum of a large bandwidth is often demanded to enhance longitudinal coherence and spectral purity at the experiment. In the hard X-ray range cryo-cooled silicon crystal monochromators are widely used at 3rd generation synchrotron sources [7-9]. Due to uniqueness of the European XFEL facility generating high-intensity X-ray pulses (10^{12} photons/pulse) of less than 100 fs duration at MHz repetition rates the performance of crystal optics is less studied than at synchrotrons. Recent studies have revealed significant heat bump effects affecting silicon monochromator optics and impairing intra-train transmission under extreme heat load conditions produced by MHz XFEL pulse trains [10]. High thermal conductivity, low thermal expansion and radiation hardness make diamond crystals very attractive for X-ray optics

applications at modern synchrotrons and XFELs [11]. During last decade significant progress has been achieved in diamond crystal growth and laser machining technologies making diamond monochromator crystals available [12, 13]. However, practical implementation of diamond optics is hindered by the available crystal quality, sizes, difficulties in mechanical processing and associated costs. In this regard, conventional silicon crystal optics has well-established fabrication technology and remains valid for a range of optical components working in hard X-ray range. In this paper we report on optical parameters, design and performance of cryogenically cooled Si111 and Si220 monochromators operational at the MID instrument of EuXFEL.

2. Experimental

2.1 MID layout

Schematic layout of the MID instrument including some of optical components in photon tunnels is shown in Fig. 1. XFEL radiation is generated in the SASE2 undulator section consisting of 35 undulator cells with total magnetic length of 175 m. The SASE beam has a very small divergence of a few microradians but due to a long propagation distance the beam size at the experimental station can easily exceed 1 mm. To provide an efficient beam transport by matching optical apertures of downstream components the SASE beam is typically collimated using a compound refractive lens (CRL) optics installed in the SASE2 tunnel (XTD1). Further beam transport is accomplished by offset X-ray mirrors M1 and M2 located in the photon tunnel (XTD6) which provide a horizontal offset of 25 mm from the direct beam path, thus eliminating forward spontaneous radiation and higher harmonics. The Si111 monochromator (Mono-1) is located at the end of XTD6 tunnel at 929 m from the undulator source. The Mono-1 can be aligned using an imager device (MID pop-in) located at 937 m and equipped with YAG and diamond screens viewed by a Basler camera [14]. A second monochromator using Si220 crystals (Mono-2) is installed further downstream in the Optics Hutch (OH) of MID at 946 m. Mono-2 enables higher energy resolution and non-dispersive diffraction conditions for split-and-delay line optics based on Si220 crystals [6]. Alignment of the Mono-2 is accomplished using OH pop-in imager device placed at 2.5 m distance downstream the monochromator. After OH the beam enters the MID experimental hutch (EH) where it reaches the sample position in the multi-purpose chamber (MPC) at 959 m. The forward transmitted beam can be imaged by the YAG screen integrated in the diagnostic endstation (DES) [15] placed at the end of MID EH.

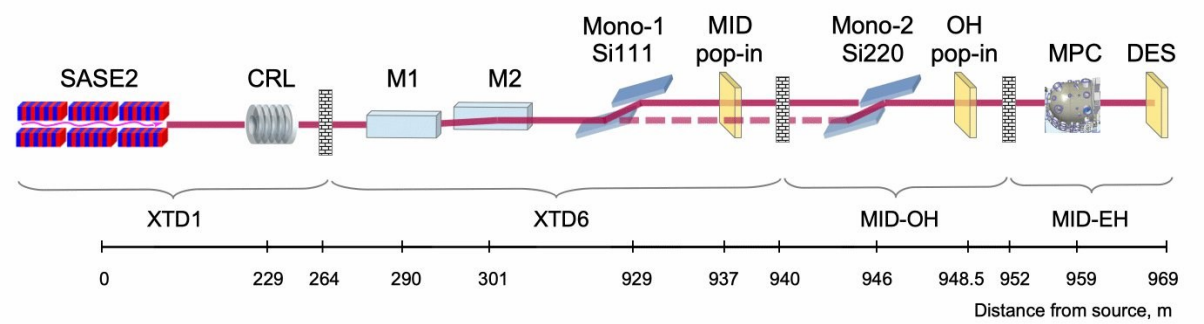

Figure 1. Schematic layout of the MID instrument.

2.2 Monochromator design

Optomechanical design of the monochromator (Fig. 2) is based on an artificial channel-cut monochromator (ACCM) concept [16, 17] employing two silicon crystals separated by a gap and

positioned to diffract in a vertical plane. In this case, each crystal surface can be polished individually before being mounted in the crystal cage, providing superior surface finish and thus preserving coherence of the beam wavefront. The channel-cut geometry results in a vertical offset of the exit beam relative to the incident beam height, varying as a function of operation energy, i.e. it is not a fixed-exit mechanics. Geometrical parameters of silicon crystals (Crystal Scientific)

Table 1. Geometrical parameters of ACCM monochromators.

Crystal pair	Dimensions L×H×W, mm³		Gap, mm	Vertical beam offset, mm			Bragg angle range, deg.
	1st crystal	2nd crystal		5 keV	9 keV	25 keV	
Si111	60×20.5×28	60×20.5×22	5.9	10.8	11.5	11.8	4.5–23.3
Si220			7.8	11.9	14.5	15.5	7.4–40.2

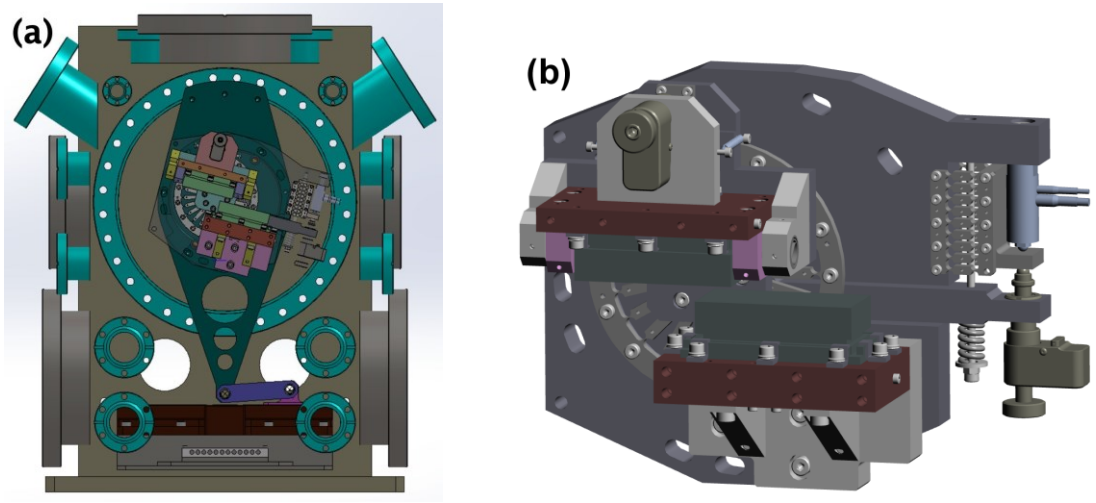

Figure 2. Technical drawings of ACCM monochromator: (a) front view of the vacuum chamber showing internal mechanics, (b) ACCM crystal holder stage. On both plots the beam direction is from right to left.

and their settings for both monochromators are given in Table 1.

Design drawing of the ACCM stage is shown in Fig. 2b. The first (bottom) crystal is mechanically clamped to a copper block which is rigidly mounted to the base plate with a PEEK spacer in between assuring thermal isolation under cryogenic conditions. The ACCM stage is mounted to a large rotation bearing enabling Bragg angle alignment by means of a sine bar mechanics (Fig. 2a). The sine bar is driven by an in-vacuum high precision linear translation equipped with encoder (PI Micos PLS-85) that provides a total stroke of 155 mm (Table 2). The monochromator design enables a total angular range of Bragg rotation of 35 deg. The second (top) crystal requires roll and pitch angular adjustments for a parallel alignment of diffraction planes between both crystals. To enable a roll motion the second crystal holder has a mechanical bearing which can be tilted by a picomotor actuator (Newport) providing a sufficient angular range. A circular torsion structure is integrated to the base plate that enables a pitch angular tilt of a second crystal. Coarse adjustment of a pitch angle is accomplished by a picomotor actuator attached to the lever arm of a circular torsion spring. To change a coarse pitch of a top crystal in one direction the actuator elongates and pushes against a compression spring. Backwards tilt is achieved by

contracting motion of an actuator assisted by a compression spring force. Fine pitch adjustment in a narrow angular range of 150 μrad is performed by a high-precision piezo actuator (PI P-841, 15 μm travel range) acting against a linear flexure which holds the flat interface adapter in between the picomotor's and piezo actuator's ball heads. Cryo-cooling of both monochromator crystals is provided indirectly by copper braids mechanically attached to the copper block of a crystal holder at one end and to a cold finger at an other end. Cryogenic operation is supplied by a pulse tube closed-loop helium cryo-compressor (Cryomech PT-60) with a cooling capacity of 60W at 80K. The copper blocks of both crystal holders are equipped with heaters and PT100 sensors to enable temperature control.

Monochromator crystals and mechanical assembly are enclosed in UHV chamber equipped

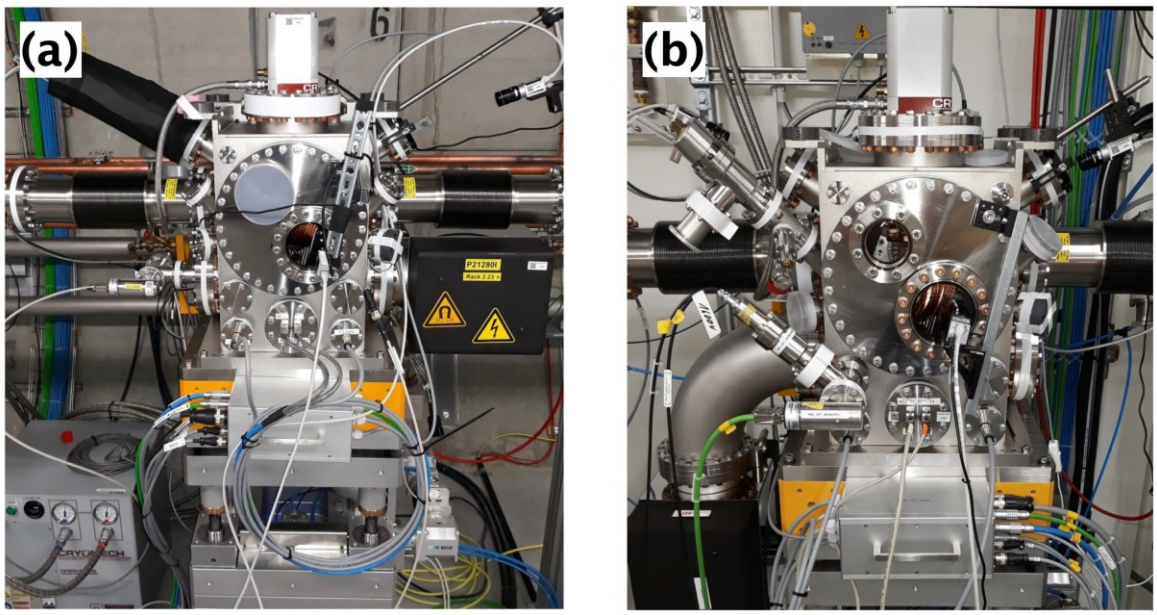

Figure 3. Photographs of (a) Si111 monochromator located at XTD6 photon tunnel and (b) Si220 monochromator installed at OH of MID.

Table 2. Angular and linear motions of ACCM monochromators.

Motion	ACCM pitch (sine bar)	Coarse pitch (picomotor)	Roll (picomotor)	Fine pitch (PI piezo)	TX	TY
Function	Bragg angle (both crystals)	Coarse pitch (2nd crystal)	Roll (2nd crystal)	Fine pitch (2nd crystal)	Horizontal translation	Vertical translation
Travel range	35 deg. (155 mm)	±10 mrad (±1 mm)	100 mrad (5 mm)	150 µrad (15 µm)	40 mm	30 mm
Resolution	0.05 µm	5 µm	5 µm	1 µrad	1 µm	1 µm

with feedthrough flanges for cabling and viewport flanges for auxiliary diagnostics components. The chamber is mounted on a motorised support table (Huber Diffraktionstechnik) providing horizontal and vertical translations for the transverse alignment of monochromator optics in the beam. Fig. 3 shows Si111 and Si220 monochromators at their locations in a photon tunnel and OH of MID instrument, respectively.

2.3 Monochromator alignment

The alignment of an ACCM monochromator consists of several steps. By design, the bottom crystal has a larger physical width than the top crystal thus providing a free edge of about 3 mm for the alignment of a single-bounce reflection satisfying the exact Bragg angle at a given photon energy. The reflected beam from a first crystal can be detected using a large-area YAG screen attached to the angled viewport flange and a Basler camera with objective lens providing an image of reflected beam cross-section. Once the reflection from a first crystal is aligned the monochromator can be fully translated into the beam path for the alignment of a second reflection from top crystal using its roll and tilt angular motions. The double-bounce reflection can be viewed at the downstream pop-in imager (MID pop-in for Mono-1 and OH pop-in for Mono-2) and is vertically offset from the incident beam position. Vertical offset is a function of Bragg angle and a gap between two crystal surfaces. Beam offset values corresponding to 5, 9 and 25 keV X-ray energies are listed in Table 1 for both monochromators. Depending on mutual pre-alignment and miscut angles of monochromator crystals the alignment of roll and pitch (coarse and fine) angles of a second crystal has to be accomplished within accessible range. Energy selection is performed by scanning Bragg angle (ACCM scan) of both crystals over a spectral bandwidth of XFEL beam.

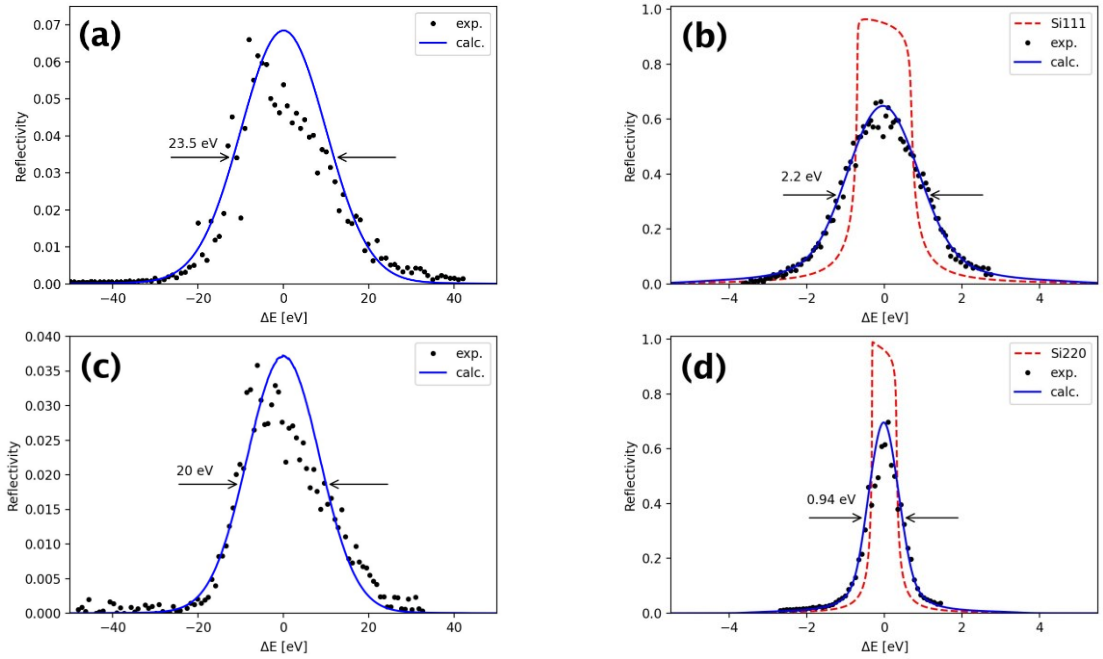

Figure 4. (a,c) Energy scans and (b,d) diffraction curves by 2nd crystal of Si111 (a,b) and Si220 (c,d) monochromator optics. Experimental data are displayed by dots. Solid blue lines represent calculated curves using dynamical diffraction theory. Dashed red lines in (b,d) denote Bragg reflectivity curves from a perfect Si crystal.

3. Results and discussion

Measurements were conducted at the MID instrument using SASE XFEL beam in single bunch mode collimated by CRL optics. Temperature of monochromator crystals was set to 100 K and X-ray photon energies of 10.5 keV and 11 keV were used for Si111 and Si220 monochromators, correspondingly. Fig. 4 shows diffraction curves obtained in energy scanning mode (ACCM angle scan of both crystals) and rocking curves by a second crystal (fine pitch scan) for Si111 (a,b) and

Si220 (c,d) monochromators. Experimental data were fitted by calculated curves using dynamical diffraction profile convolved with spectral bandwidth modelled by a gaussian shape. The obtained energy scans provide a direct measure of SASE spectral bandwidth and have revealed full width at half-maximum (FWHM) values of 23.5 eV at maximum reflectivity of 6.8% in case of Si111 monochromator and 20 eV at maximum reflectivity of 3.7% for Si220 optics. The observed difference in SASE bandwidths can be due to different XFEL machine settings applied during corresponding beamtimes. Experimental ACCM curves show slightly asymmetric shape indicating more complex shape of SASE spectral distribution than a gaussian. Diffraction curves performed using a second monochromator crystal (fine pitch scan) represent essentially analyser crystal scans and enable to determine the spectral bandwidth selected by the first monochromator crystal. Fine pitch scans and their fitting curves are presented in Fig. 4 (b,d) and the obtained FWMH values of 2.2 eV for Si111 optics and 0.94 eV for Si220 monochromator are in agreement with design characteristics [5].

4. Summary

Optical parameters and design of cryo-cooled silicon monochromators implemented at the MID instrument of the European XFEL are described. Both devices are based on ACCM concept using Si111 and Si220 crystal pairs and can be used in 5–25 keV photon energy range. Performance results confirm energy selectivity and stability of monochromators operating with SASE XFEL beam. An extended range towards harder X-rays (above 30 keV) can be accessed using higher order reflections such as Si333 and Si440 which is suitable for future high-harmonic lasing operation of the EuXFEL.

Acknowledgements

We thank X. Dong for assembly of monochromator components and K. Sukharnikov for electrical controls support. G. Ansaldi, A. Bartmann, M. Neumann, B. Rio and A. Schmidt are thanked for technical support. Metrology measurements by I. Freijo-Martin, J. Heuer, and H. Schulte_Schrepping are gratefully acknowledged.

References

[1] Emma, P. *et al*. Nat. Photon. **4**, 641–647 (2010)
[2] Ishikawa, T. *et al.* Nat. Photon. **6**, 540–544 (2012)
[3] Decking, W., *et al.* Nat. Photon. **14**, 391–397 (2020)
[4] Tschentscher, T., Bressler, C., Gruenert, J., Madsen, A., Mancuso, A. P., Meyer, M., Scherz, A., Sinn, H. & Zastrau, U. Appl. Sci. **7**, 592 (2017)
[5] Madsen, A., Hallmann, J., Roth, T. and Ansaldi, G. (2013). Technical Design Report: Scientific Instrument MID, Technical Report XFEL.EU TR-2013-005. European X-ray Free Electron Laser, Hamburg, Germany
[6] Madsen, A., et al. J. Synchrotron Rad. **28**, 637–649 (2021)
[7] Ishikawa, T., Tamasaku, K., Yabashi, M. Nucl. Instr. and Meth. A **547**, 42–49 (2005)
[8] Toellner, T. S., Alatas, A., Said, A., Shu, D., Sturhahn, W. and Zhao, J. J. Synchrotron Rad. **13**, 211–215 (2006)
[9] Zozulya, A. V., Shabalin, A., Schulte-Schrepping, H., Heuer, J., Spiwek, M., Sergeev, I., Besedin, I., Vartanyants, I. A. and Sprung, M. J. Phys.: Conf. Ser. **499**, 012003 (2014)
[10] Petrov, I., *et al*. Opt. Express **30,** 4978–4987 (2022)
[11] Shvyd'ko, Y., Blank, V., Terentyev, S. MRS Bulletin **42**, 437–444 (2017)
[12] Shvyd'ko, Y., Terentyev, S., Blank, V., Kolodziej, T. J. Synchrotron Rad. **28**, 1720–1728 (2021)
[13] Tasca, K. R., Madsen, A., Petrov, I., Rodriguez-Fernandez, A., Shayduk, R., Vannoni, M., Zozulya, A. and Samoylova, L. Proc. SPIE Vol. **12581**, 125810L (2023)
[14] Koch, A., Risch, J., Freund, W., Maltezopoulos, T., Planas, M. and Gruenert, J. J. Synchrotron Rad. **26**, 1489–1495 (2019)
[15] Boesenberg, U. et al. J. Synchrotron Rad. **31**, 596–604 (2024)
[16] Shu, D., Toellner, T.S., Alp, E.E. Nucl. Instrum. Methods A 467-468 (1), 771–774 (2001)
[17] Dong, X., Shu, D., and Sinn, H. AIP Conference Proceedings **1741**, 040027 (2016)